JMEPEG (2014) 23:2943–2952
DOI: 10.1007/s11665-014-1052-2

1059-9495/$19.00

Growth Kinetics of the Fe_2B Layers and Adhesion on Armco Iron Substrate

M. Elias-Espinosa, M. Ortiz-Domínguez, M. Keddam, M.A. Flores-Rentería, O. Damián-Mejía, J. Zuno-Silva, J. Hernández-Ávila, E. Cardoso-Legorreta, and A. Arenas-Flores

(Submitted January 17, 2014; in revised form February 19, 2014; published online May 24, 2014)

In this work, a kinetic model was suggested to evaluate the boron diffusion coefficient in the Fe_2B layers grown on the Armco iron substrate by the powder-pack boriding. This thermochemical treatment was carried out in the temperature range of 1123-1273 K for treatment times ranging from 2 to 8 h. The boron diffusion coefficient in the Fe_2B layers was estimated by solving the mass balance equation at the (Fe_2B/substrate) interface with an inclusion of boride incubation time. To validate the present model, the simulated value of Fe_2B layer thickness was compared with the experimental value obtained at 1253 K for a treatment time of 5 h. The morphology of Fe_2B layers was observed by SEM and optical microscopy. Metallographic studies showed that the boride layer has a saw-tooth morphology in all the samples. The layer thickness measurements were done with the help of MSQ PLUS software. The Fe_2B phase was identified by x-ray diffraction method. Finally, the adherence of Fe_2B layers on the Armco iron substrate was qualitatively evaluated by using the Daimler-Benz Rockwell-C indentation technique. In addition, the estimated value of boron activation energy was compared to the literature data.

Keywords activation energy, adherence, boriding, diffusion model, growth kinetics

1. Introduction

The boriding process is a thermochemical surface hardening process that modifies a material surface by the diffusion of boron atoms into the surface layer at high temperatures. As a result, the boriding processes enhance the surface hardness and wear resistance of ferrous alloys.

The boriding treatment can be performed in numerous ways, including plasma, salt bath, paste and pack-boriding techniques (Ref 1). The most frequently used method is pack boriding which is similar to pack carburizing process (Ref 2, 3). The powder-pack boriding is technologically, simpler and more economic in comparison with other boriding processes (Ref 4).

The boriding of ferrous materials results in the formation of the Fe_2B layer or double layer (FeB/Fe_2B) with definite

Nomenclature

v	Boride layer thickness (m)
t_v	is the effective growth time of the Fe_2B layer (s)
t	is the treatment time (s)
$t_0^{Fe_2B}$	is the boride incubation time (s)
Q_{Fe_2B}	the boron activation energy (J/mol)
$C_{up}^{Fe_2B}$	represents the upper limit of boron content in Fe_2B ($=60 \times 10^3$ mol/m^3)
$C_{low}^{Fe_2B}$	is the lower limit of boron content in Fe_2B($=59.8 \times 10^3$ mol/m^3)
C_{ads}^{B}	is the adsorbed boron concentration in the boride layer (mol/m^3)
$a_1 = C_{up}^{Fe_2B} - C_{low}^{Fe_2B}$	defines the homogeneity range of the Fe_2B layer (mol/m^3)
$a_2 = C_{low}^{Fe_2B} - C_0$	is the miscibility gap (mol/m^3)
C_0	is the terminal solubility of the interstitial solute (≈ 0 mol/m^3)
$C_{Fe_2B}[x(t)]$	is the boron concentration profile in the Fe_2B layer (mol/m^3)
v_0	indicates the initial Fe_2B layer (m)
ε	is the normalized growth parameter for the (Fe_2B/substrate) interface (it has no physical dimensions)
D_{Fe_2B}	denotes the diffusion coefficient of boron in the Fe_2B phase (m^2/s)
$J_i[x(t)]$, (with $i = Fe_2B$ and Fe)	are the fluxes of boron atoms in the (Fe_2B/substrate) interface boundary (mol/m^2/s)

M. Elias-Espinosa, Instituto Tecnológico y de Estudios Superiores de Monterrey-ITESM Campus Santa Fe, Av. Carlos Lazo No. 100, Del. Álvaro Obregón, 01389 Mexico, DF, Mexico; **M. Ortiz-Domínguez** and **J. Zuno-Silva**, Universidad Autónoma del Estado de Hidalgo, Campus Sahagún, Carretera Cd. Sahagún-Otumba s/n, Pachuca de Soto, Hidalgo, Mexico; **M. Keddam**, Laboratoire de Technologie des Matériaux, Faculté de GénieMécanique et Génie des Procédés, USTHB, B.P. No. 32, El-Alia, Bab-Ezzouar, 16111 Algiers, Algeria; **M.A. Flores-Rentería**, Universidad Politécnica de Pachuca-UPP, Carretera Pachuca-Cd. Sahagún km. 20, Ex Hacienda de Santa Bárbara, 43830 Zempoala, Hidalgo, Mexico; **O. Damián-Mejía**, Instituto de Investigación en Materiales, Universidad Nacional Autónoma de México-UNAM, Circuito Exterior, s/n Ciudad Universitaria, Coyoacán, 04510 Mexico, DF, Mexico; and **J. Hernández-Ávila, E. Cardoso-Legorreta,** and **A. Arenas-Flores**, Centro de Investigaciones en Materiales y Metalurgia, Universidad Autónoma del Estado de Hidalgo, Ciudad Universitaria Pachuca-Tulancingo km. 4.5, Pachuca, Hidalgo, Mexico. Contact e-mail: keddam@yahoo.fr.

composition (Ref 5-8). The Fe_2B phase contains 59.2×10^3 mol/m^3 of boron (Ref 9), while the FeB phase has a boron composition of 100×10^3 mol/m^3 (Ref 10). The FeB phase is brittle and forms a surface that is under high-tensile stress. The Fe_2B phase is preferred because it is less brittle than FeB and forms a surface with a high-compressive stress.

In the literature, several models were reported to study the growth kinetics of Fe_2B layers grown on different substrates (Ref 11-20) with and without the boride incubation times.

The main objective of this study was to investigate the mechanical property in terms of interfacial cohesion and diffusion kinetics of Fe_2B layers formed on Armco iron.

A diffusion model was also suggested to evaluate the boron diffusion coefficient in the Fe_2B layers on Armco iron substrate in the temperature range of 1123-1273 K. The estimated boron activation energy of borided Armco iron was then compared to the literature data.

The model was validated by predicting the Fe_2B layer thickness obtained at a temperature of 1253 K for 5 h.

2. The Diffusion Model

The model considers a diffusion of boron atoms into a saturated substrate by forming the Fe_2B layer. There is no boron flux out of the surface layer of Fe_2B into the Fe matrix. The boron concentration profile through the Fe_2B layer is displayed in Fig. 1.

At the beginning, the boron atoms diffuse into the iron lattice to form a saturated solid solution. The boron concentration profile is described by $f(x, t)$. After exceeding the boride incubation time $t_0^{Fe_2B}$, the Fe_2B layer begins to form and becomes continuous and more compact after a prolonged time. $C_{up}^{Fe_2B}$ denotes the upper limit of boron content in Fe_2B(=60×10^3 mol/m^3), $C_{low}^{Fe_2B}$ is the lower limit of boron content in Fe_2B(=59.8×10^3 mol/m^3), and the point $x(t = t) = v$ represents the Fe_2B layer thickness. The boron concentration $\left(C_{Fe_2B}[x(t), t] = A + B\,\mathrm{erf}(x/\sqrt{4D_{Fe_2B}t})\right)$ in the Fe_2B layer (see Fig. 1) is the solution of Fick's Second Law in a semi-infinite medium, and it depends on the position $x(t)$ and t time [cf. the small homogeneity ranges of about 1 at.% for the Fe_2B layer (Ref 10)]. Further assuming that the boron surface and interface concentration do not change during boriding process.

A schematic representation of the $C_{up}^{Fe_2B}$ and $C_{low}^{Fe_2B}$ values obtained from the Fe-B phase diagram for a range of temperatures is given in Fig. 2.

The term C_{ads}^{B} is the effective boron concentration or adsorbed boron concentration in the boride layer during the boriding process (Ref 21). From Fig. 1, $a_1 = C_{up}^{Fe_2B} - C_{low}^{Fe_2B}$ denotes the homogeneity range of the Fe_2B layer, $a_2 = C_{low}^{Fe_2B} - C_0$ is the miscibility gap, and C_0 is the boron solubility in the matrix. The diffusion zone in the substrate underneath the compound layer can be ignored ($C_0 \approx 0$ mol/m^3) (Ref 22, 23).

The following assumptions are considered for the diffusion model:

- The growth kinetics is controlled by the boron diffusion in the Fe_2B layer.
- The Fe_2B iron boride nucleates after a specific incubation time.
- The boride layer grows because of the boron diffusion perpendicular to the specimen surface.
- Boron concentrations remain constant in the boride layer during the treatment.
- The influence of the alloying elements on the growth kinetics of the layer is not taken into account.
- The boride layer is thin compared to the sample thickness.
- A uniform temperature is assumed throughout the sample.
- Planar morphology is assumed for the phase interface.

The initial and boundary conditions for the diffusion problem are represented as follows:

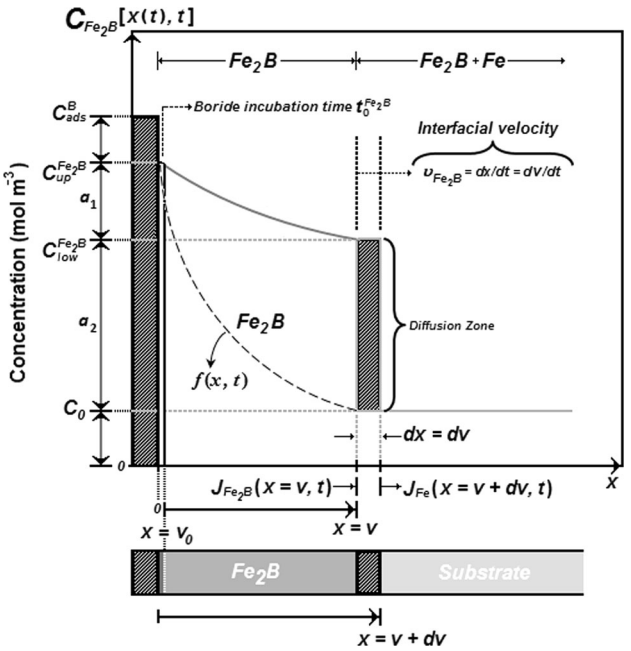

Fig. 1 Boron concentration profile through the Fe_2B layer

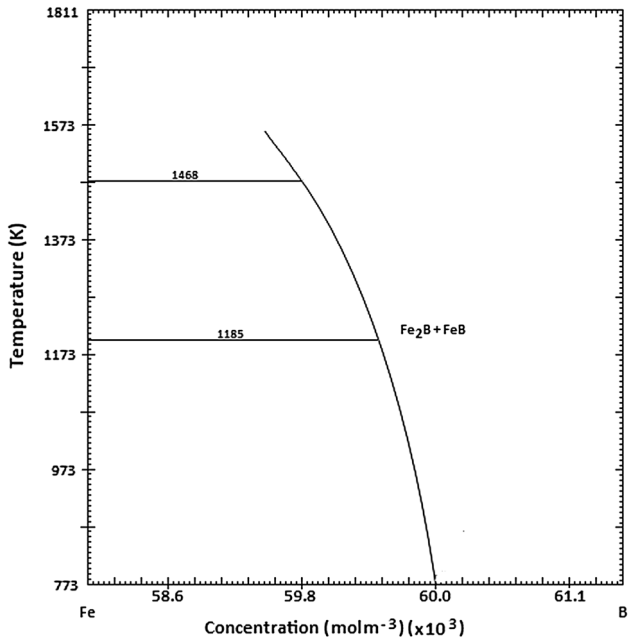

Fig. 2 Schematic representation of the $C_{up}^{Fe_2B}$ and $C_{low}^{Fe_2B}$ values obtained from the Fe-B phase diagram for a range of temperatures

$$t = 0, x > 0, \text{ with: } C_{Fe_2B}[x(t), t = 0] = C_0 \approx 0. \quad \text{(Eq 1)}$$

Boundary conditions:

$$\left.\begin{array}{l} C_{Fe_2B}\left[x\left(t = t_0^{Fe_2B}\right) = v_0, t = t_0^{Fe_2B}\right] = C_{up}^{Fe_2B} \\ \text{(the upper boron concentration is kept constant),} \\ \text{for } C_{ads}^{B} > 60 \times 10^3 \text{ mol/m}^3, \end{array}\right\} \quad \text{(Eq 2)}$$

$$\left.\begin{array}{l} C_{Fe_2B}[x(t = t) = v, t = t] = C_{low}^{Fe_2B} \\ \text{(the boron concentration at the interface is kept constant),} \\ C_{ads}^{B} < 59.8 \times 10^3 \text{ mol/m}^3, \end{array}\right\} \quad \text{(Eq 3)}$$

v_0 is a thin layer with a thickness of ≈5 nm that formed during the nucleation stage (Ref 24). Thus, $v_0(\approx 0)$ when compared to the thickness of Fe_2B layer (v). The mass balance equation (Ref 25, 26) at the (Fe_2B/substrate) interface can be formulated by Eq 4 as follows:

$$\left(\frac{C_{up}^{Fe_2B} + C_{low}^{Fe_2B} - 2C_0}{2}\right)(A \cdot dv) = J_{Fe_2B}(x = v, t = t)\,(A \cdot dt) - J_{Fe}(x = v + dv, t = t)\,(A \cdot dt), \quad \text{(Eq 4)}$$

where $A\,(= 1 \cdot 1)$ is defined as the unit area and C_0 represents the boron concentration in the matrix. The flux J_{Fe_2B} and J_{Fe} are obtained from the Fick's First law as

$$J_{Fe_2B}[x(t = t) = v, t = t] = -\{D_{Fe_2B}\partial C_{Fe_2B}[x(t = t) = v, t = t]/\partial x\}_{x = v}, \quad \text{(Eq 5)}$$

and

$$J_{Fe}[x(t = t) = v + dv, t = t] = -\{D_{Fe}\partial C_{Fe}[x(t = t) = v + dv, t = t]/\partial x\}_{x = v + dv}. \quad \text{(Eq 6)}$$

The term J_{Fe} is null, since the boron solubility in the diffusion zone is very low (≈0 mol/m^3) (Ref 3).

Thus, Eq 4 can be written as

$$\left(\frac{C_{up}^{Fe_2B} + C_{low}^{Fe_2B} - 2C_0}{2}\right)\left.\frac{dx(t)}{dt}\right|_{x(t) = v} = -D_{Fe_2B}\left.\frac{\partial C_{Fe_2B}[x(t = t), t = t]}{\partial x}\right|_{x(t) = v}. \quad \text{(Eq 7)}$$

If the boron concentration profile in Fe_2B is constant for the treatment time, Fick's Second law is reduced to an ordinary second-order differential equation as follows:

$$\frac{\partial C_{Fe_2B}[x(t), t]}{\partial t} = D_{Fe_2B}\frac{\partial^2 C_{Fe_2B}[x(t), t]}{\partial x^2}. \quad \text{(Eq 8)}$$

By solving Eq 8, and applying the boundary conditions proposed in Eqs 2 and 3, the boron concentration profile in Fe_2B is expressed by Eq 9 if the boron diffusion coefficient in Fe_2B is constant for a particular temperature

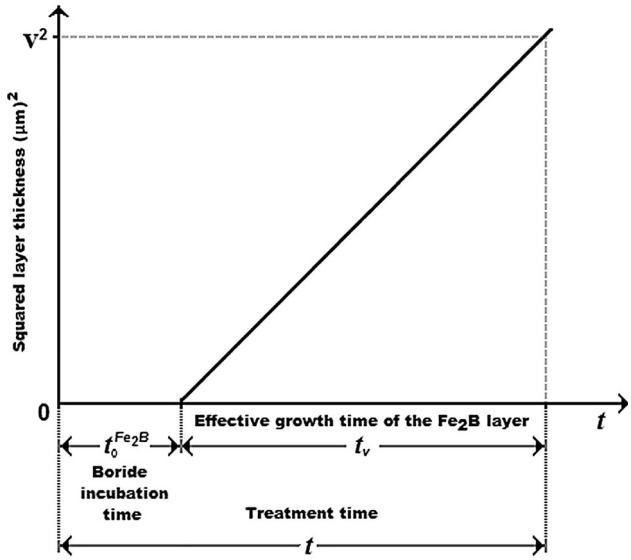

Fig. 3 A Schematic representation of the square of the layer thickness as a function of treatment time

$$C_{Fe_2B}[x(t), t] = C_{up}^{Fe_2B} + \frac{C_{low}^{Fe_2B} - C_{up}^{Fe_2B}}{\operatorname{erf}\left(\frac{v}{2\sqrt{D_{Fe_2B}t}}\right)}\operatorname{erf}\left(\frac{x}{2\sqrt{D_{Fe_2B}t}}\right). \quad \text{(Eq 9)}$$

By substituting Eq 9 into Eq 7, Eq 10 is obtained

$$\left(\frac{C_{up}^{Fe_2B} + C_{low}^{Fe_2B} - 2C_0}{2}\right)\frac{dv}{dt} = \sqrt{\frac{D_{Fe_2B}}{\pi t}}\frac{C_{up}^{Fe_2B} - C_{low}^{Fe_2B}}{\operatorname{erf}\left(\frac{v}{2\sqrt{D_{Fe_2B}t}}\right)}\exp\left(-\frac{v^2}{4D_{Fe_2B}t}\right), \quad \text{(Eq 10)}$$

for $0 \le x \le v$.

Substituting the expression of the parabolic growth law ($v = 2\varepsilon D_{Fe_2B}^{1/2} t^{1/2}$) into Eq 10, Eq 11 is deduced

$$\left(\frac{C_{up}^{Fe_2B} + C_{low}^{Fe_2B} - 2C_0}{2}\right)\varepsilon = \sqrt{\frac{1}{\pi}}\frac{C_{up}^{Fe_2B} - C_{low}^{Fe_2B}}{\operatorname{erf}(\varepsilon)}\exp(-\varepsilon^2). \quad \text{(Eq 11)}$$

The normalized growth parameter (ε) for the (Fe_2B/substrate) interface can be estimated numerically by the Newton-Raphson method. It is assumed that expressions $C_{up}^{Fe_2B}$, $C_{low}^{Fe_2B}$, and C_0 do not depend significantly on temperature (in the considered temperature range) (Ref 10).

A schematic representation of the square of the layer thickness against linear time ($v^2 = 4\varepsilon^2 D_{Fe_2B} t = 4\varepsilon^2 D_{Fe_2B}\left(t_v + t_0^{Fe_2B}\right)$) is depicted in Fig. 3. $t_v\left(= t - t_0^{Fe_2B}\right)$ is the effective growth time of the Fe_2B layer and t is the treatment time.

3. Mechanism of Formation of the Fe_2B Layer

In the powder-pack boriding process, the diffusion of boron atoms in the direction of the substrate gives rise to the

formation of hard phases known as the iron borides in case of ferrous alloys. The appearance of these phases in the borided case is related to change in the boron concentration profile. The overall chemical reaction given by Eq 12 takes place during the powder-pack boriding process

$$B_4C + 4KBF_4 + 3SiC + 2O_2 \rightarrow 8B\ (\text{adsorption}) + 4KF + 3SiF_4 + 4CO. \quad (\text{Eq } 12)$$

Since the presence of oxygen promotes oxidation of active boron Eq 13 becomes

$$B_4C + 4KBF_4 + 3SiC + 3O_2 \rightarrow 6B\ (\text{adsorption}) + 4KF + 3SiF_4 + 4CO + B_2O_2. \quad (\text{Eq } 13)$$

In this thermochemical treatment, the diffusion of atomic boron is mainly influenced by the contact surface between the boriding agent and the substrate. The boriding powder with finer sizes allows for better diffusion of boron atoms into the material substrate.

The diffusion of boron atoms leads to a saturation of the iron matrix. After exceeding a certain period of incubation, the Fe_2B layer forms if the boron concentration is within the composition range of $C_{low}^{Fe_2B} < C_{up}^{Fe_2B} < C_{ads}^{B}$ and the following chemical reaction occurs

$$B\ (\text{adsorption}) + 2Fe \rightarrow Fe_2B. \quad (\text{Eq } 14)$$

Nucleation of iron boride at the gas-solid interface is the net result of a competition between the supply of boron from the gas phase and the removal of boron by diffusion into the substrate. In the early stage of growth, acicular Fe_2B crystals grow in radial directions starting from the contact zones between the metal surface and boron atoms (Fig. 4), lengthening upon the surface of the base metal. These features can be explained considering that (Stage 1) only solid state reactions occurred, and consequently, active boron was supplied only at the contact zones between the metal surface and boron atoms; (Stage 2) Fe_2B crystals preferentially grow along their [001] crystallographic direction, i.e., the direction which has the shortest distance between neighboring boron atoms and, consequently, constitutes the easier path for the boron diffusion in the body-centered tetragonal lattice of Fe_2B; and (Stage 3) the Fe_2B needles growing upon the metal surface find a minimum of mechanical resistance from the base metal, because of the considerable increase in volume (~16%) associated with the transformation of Fe into Fe_2B. This kind of growth leads to the formation of a first layer of differently oriented crystals, i.e., an outermost, mechanically inconsistent layer (Ref 27).

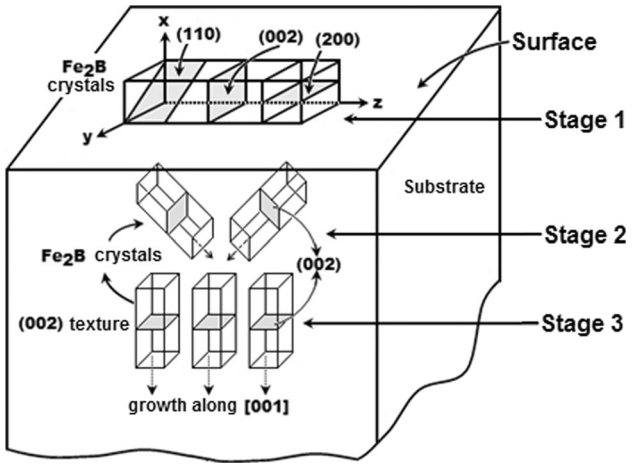

Fig. 4 Schematic representation of the stages of thermochemical growth of Fe_2B crystals: Stage 1, growth on the metal surface; Stage 2, growth inside the outer regions of the metal sample; and Stage 3, growth in depth leading to a strong (002) preferred orientation (Ref 27)

The authors Ninham and Hutchings (Ref 28) suggested that the columnar nature of the coating interface is caused by dendrite "side arm" growth similar to the growth that occurs during the solidification of many metallic systems. In borided low-carbon steels, the boride may "break through" the band of impurities in some places, which allows local rapid boride growth and results in the characteristic saw-toothed interface. A different mechanism has also been proposed in which local high stress fields and lattice distortions near the tips of the first acicular nuclei of the reaction products are assumed to be responsible to the columnar growth of borides (Ref 29).

4. Experimental Procedure

4.1 The Boriding Process

The material to be borided is ARMCO iron. This alloy has a nominal chemical composition of 0.02% C, 0.20% Mn, 0.015% P, 0.015% S, 0.007% N, and 0.06% Cu. The samples were sectioned into cubic samples with dimensions of $10 \times 10 \times 10$ mm^3.

Prior to the boriding process, the samples were polished, ultrasonically cleaned in an alcohol solution and deionized water for 15 min at room temperature, and dried and stored under clean room conditions. The samples were embedded in a closed cylindrical case (AISI 304L) as shown in Fig. 5, containing a Durborid fresh powder mixture with particles size of 50 μm.

This boriding agent is composed of B_4C as a boron source, an inert filler as SiC, and an activator as KBF_4. The active boron is then supplied by the powder quantity placed over and around the material surface.

The boriding treatment was carried in the temperature range of 1123-1273 K for a variable time (2, 4, 6, and 8 h) in a conventional furnace under a pure argon atmosphere. Once the treatment was complete, the container was removed from the furnace and slowly cooled to room temperature.

4.2 Experimental Techniques

The treated samples were cross sectioned for microstructural observations using a LECO VC-50 cutting precision machine, and the depths of the surface layers were observed in a clear field by optical microscopy using GX51 Olympus instrument. The obtained optical images were analyzed with MSQ PLUS software. The thickness measurement program is designed to measure the thickness of layers. The measurement of layer thickness is of a great importance to analyze the growth kinetics of boride layers. Automatic measurements can be performed by constructing a series of parallel section lines which are combined with the thresholded image of the layer to be measured. The lengths of those portions of the section lines which overlay the selected layer are measured. In order to minimize the roughness effect at interfaces growth, the layer thickness was defined as the average value of the long boride teeth (Ref 30-32). Fifty measurements were collected in

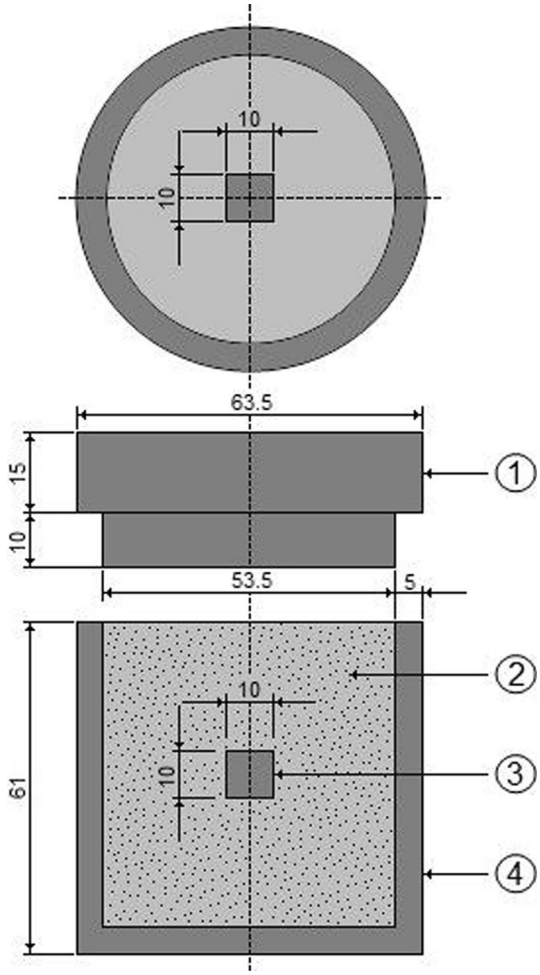

Fig. 5 Schematic view of the stainless steel AISI 304L container for the pack-powder boriding treatment (1: lid; 2: powder boriding medium (B_4C + KBF_4 + SiC); 3: sample; 4: container)

different sections of the borided samples to estimate the thickness of the Fe_2B layers.

All thickness measurements were collected from a fixed reference on the surface of the borided Armco iron, as shown in Fig. 6. The presence of the iron boride formed at the surface of borided sample was determined by means of x-ray diffraction (XRD) equipment (Equinox 2000) using CoK_α radiation at $\lambda = 0.179$ nm. The morphology of boride layers was observed by SEM (JEOL JSM 6300). The Daimler-Benz Rockwell-C cohesion test was used to assess the cohesion of the boride layers. The well-known Rockwell-C indentation test is prescribed by the VDI 3198 norm, as a destructive quality test of coated compounds (Ref 33-35). The principle of this method was given by the author Taktak (Ref 35). A load of 1471 N was applied to cause coating damage adjacent to the boundary of the indentation. Three indentations were conducted for each sample and SEM examinations were employed to evaluate the test.

5. Results of the Experimental Study

5.1 Microstructural Observations of Boride Layers

Figure 7 shows the optical images of the cross sections of borided samples at 1273 K during 2, 4, 6, and 8 h. The needles of Fe_2B boride are visible on the optical micrographs, exhibiting a saw-tooth morphology at the (Fe_2B/substrate) interface. Figure 8 gives the SEM micrograph of cross section of borided Armco iron at a temperature of 1223 K for 2 h. The Fe_2B layer is on top of the substrate where the boride needles are visible and different in length.

5.2 X-Ray Diffraction Analysis

The Fe_2B phase was identified by XRD patterns as shown in Fig. 9 at the surface of Armco iron borided at 1273 K for 8 h. The diffraction peaks of Fe_2B phase exhibited a difference in intensities.

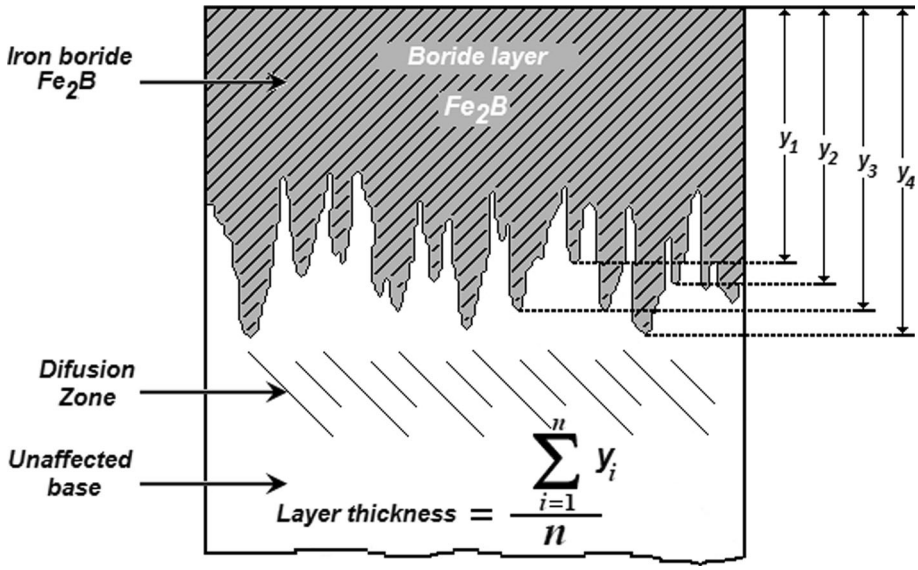

Fig. 6 Schematic representation of the Fe_2B layer measurements

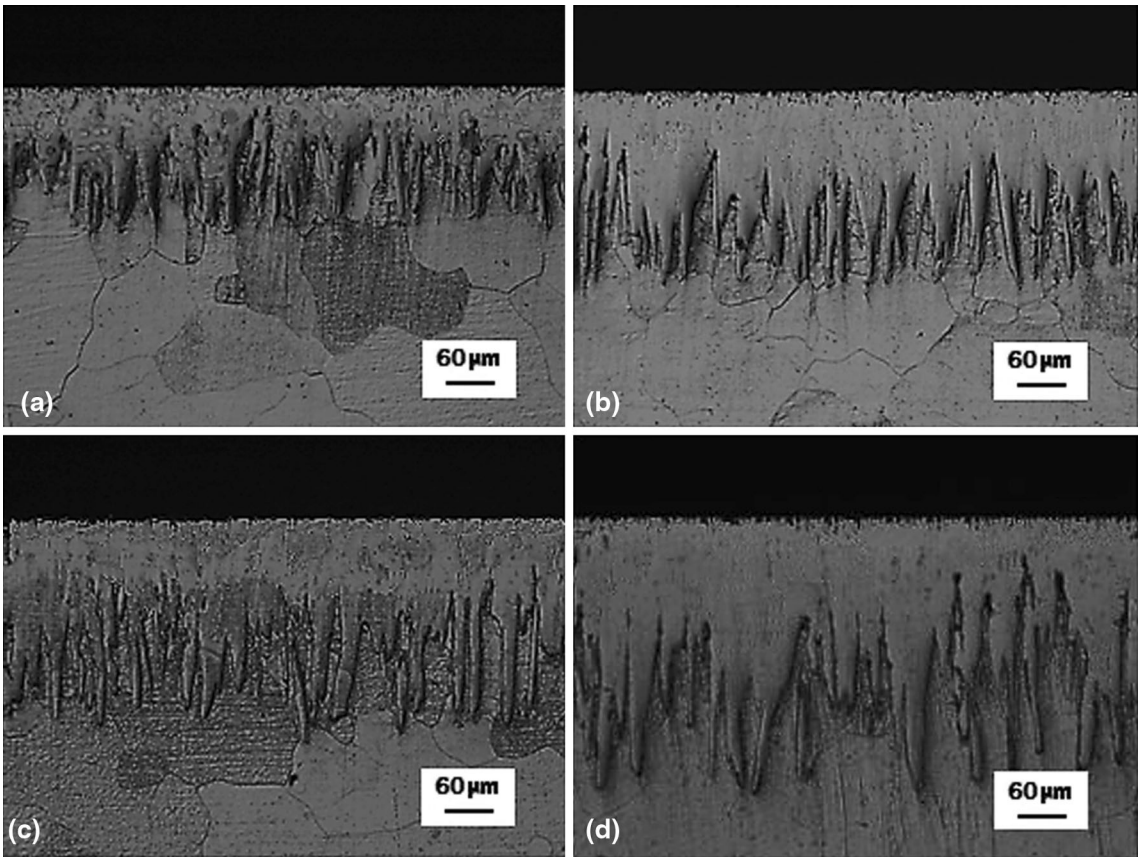

Fig. 7 Optical micrographs of the cross sections of Armco iron samples borided at 1273 K during different treatment times: (a) 2 h, (b) 4 h, (c) 6 h, and (d) 8 h

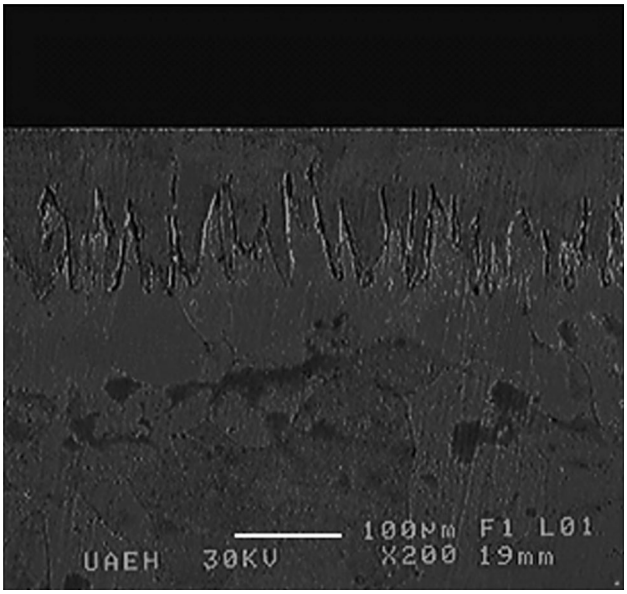

Fig. 8 SEM micrograph of the cross section of Armco iron sample borided at 1223 K during 2 h

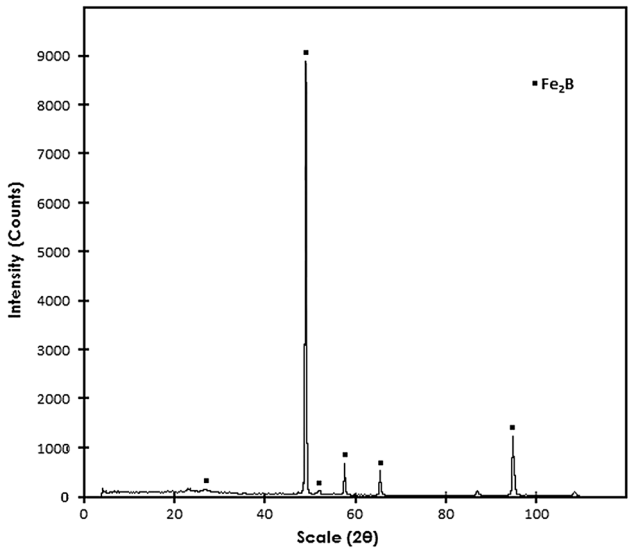

Fig. 9 XRD patterns obtained at the surface of Armco iron borided at 1273 K for 8 h

5.3 Rockwell-C Cohesion

An indenter hardness tester was employed to evaluate the Daimler-Benz Rockwell-C cohesion, as a destructive quality test for boride layers; it was employed for determination of cohesion. The well-known cohesion test prescribed by the VDI 3198 norm was used. The principle of this method is presented in Fig. 10. A conical diamond indenter penetrated into the surface of an investigated layer, thus inducing massive plastic

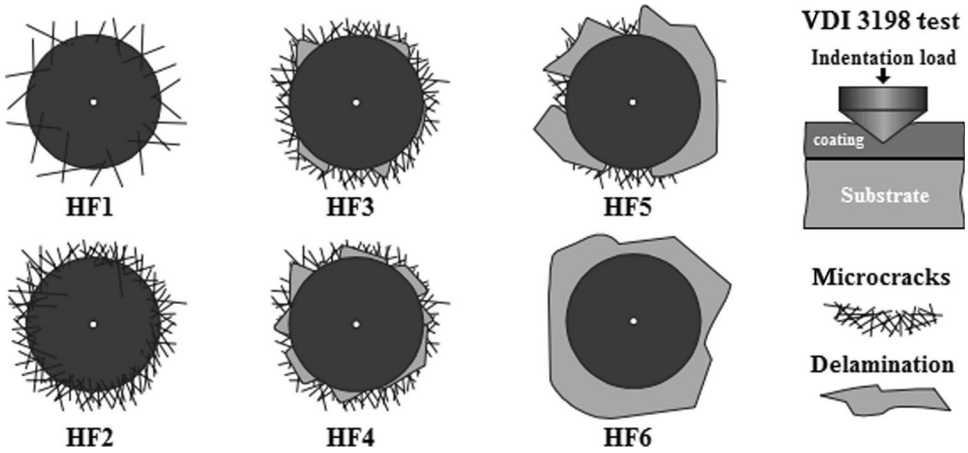

Fig. 10 Principle of the VDI 3198 indentation test (Ref 33)

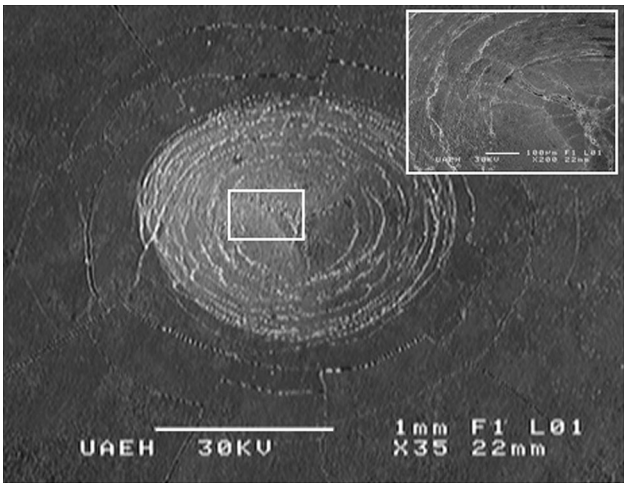

Fig. 11 SEM micrograph of the indentation crater of VDI cohesion test on the surface of Armco iron borided at 1273 K for 4 h

deformation to the substrate and fracture of the diffusion-borided layer.

The damage to the boride layer was compared with the cohesion strength quality maps HF1-HF6 (see Fig. 10). In general, the adhesion strength from HF1 to HF4 defined sufficient cohesion, whereas HF5 and HF6 represented insufficient cohesion (HF is the German short form of cohesion strength). SEM micrograph of the indentation craters for the sample borided at a temperature of 1273 K for 4 h is given in Fig. 11. The indentation craters obtained on the surface of the hardened diffusion-borided Armco iron revealed that there were radial cracks at the perimeter of indentation craters. However, a small quantity of spots with flaking of delamination was visible and the cohesion strength quality of this boride layer is related to HF4 standard.

5.4 Growth Kinetics of Fe_2B Layers

The time dependence of the square of boride layers thickness is depicted in Fig. 12. The slopes of the straight lines in this figure represent the growth constants ($= 4\varepsilon^2 D_{Fe_2B}$) of the parabolic growth law ($v^2 = 4\varepsilon^2 D_{Fe_2B} t$), where the intercept on the abscissa is taken as the boride incubation time

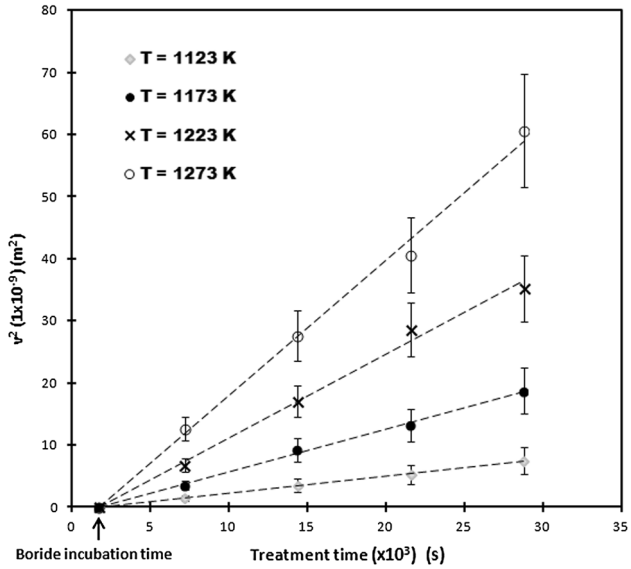

Fig. 12 Square of boride layer thickness versus the boriding time at different temperatures

Table 1 The square of normalized growth parameter and growth constants as a function of boriding temperature

Temperature, K	Type of layer	ε^2, Dimensionless	$4\varepsilon^2 D_{Fe_2B}$, $\mu m^2/s$
1123	Fe_2B	1.7471×10^{-3}	2.990×10^{-1}
1173			7.000×10^{-1}
1223			12.99×10^{-1}
1273			22.01×10^{-1}

on the graph. The results, which are summarized in Table 1, reflect a diffusion-controlled growth of the boride layers.

By combining the results [square of normalized growth parameter (ε^2) and growth constants ($4\varepsilon^2 D_{Fe_2B}$)] presented in Table 1, the boron diffusion coefficient in the Fe_2B layers (D_{Fe_2B}) was estimated for each boriding temperature. So, an Arrhenius equation relating the boron diffusion coefficient to

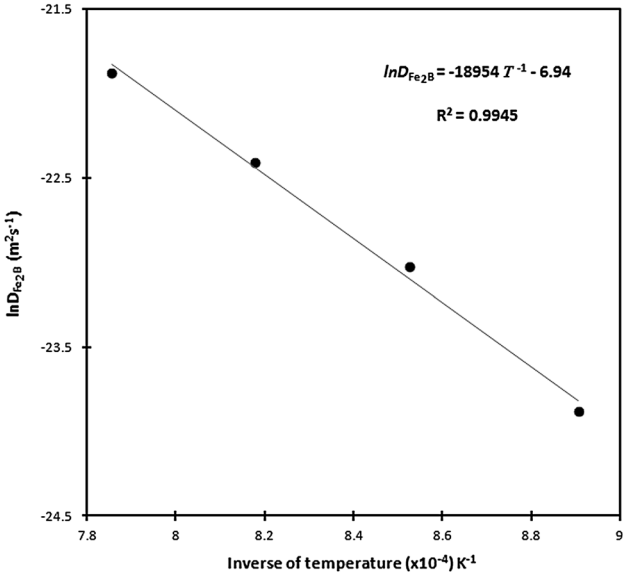

Fig. 13 Arrhenius relationship for boron diffusion coefficient through the Fe_2B layer

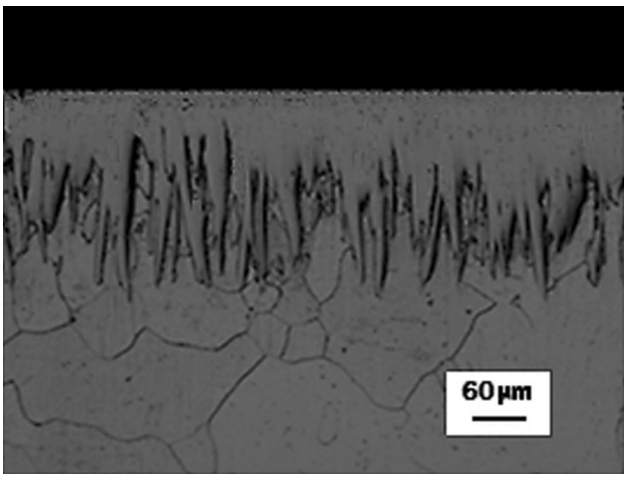

Fig. 14 Optical micrograph of the cross section of Armco iron sample borided at 1253 K during 5 h

Table 2 A comparison of the boron activation energies in the Fe_2B layers for the borided Armco iron substrates

Boriding method	Q_{Fe_2B}, kJ/mol	References
Paste	157	(12)
Paste	151	(37)
Gaseous	117.5	(38)
Gaseous	105.5	(39)
Powder	156	(10)
Powder	157.5	Present study

the boriding temperature can be adopted. As a consequence, the boron activation energy (Q_{Fe_2B}) and pre-exponential factor (D_0) can be calculated from the slopes and intercepts of the straight line shown in coordinate system: $\ln D_{Fe_2B}$ as a function of the reciprocal boriding temperature as shown in Fig. 13.

Table 3 Estimated value of the Fe_2B layer thickness (v) obtained at 1253 K during 5 h

Temperature, K	Type of layer	Boride layer thickness, µm estimated by Eq 16	Experimental boride layer thickness, µm
1253	Fe_2B	181.60	175.25 ± 12.15

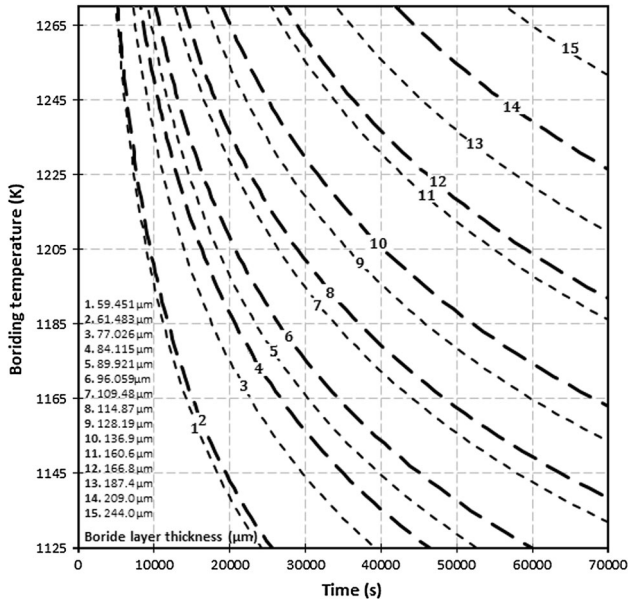

Fig. 15 Iso-thickness diagram depending on the process parameters

The boron diffusion coefficient through the Fe_2B layers was deduced as follows:

$$D_{Fe_2B} = 1.0 \times 10^{-3} \exp(-157.6\ \text{kJ/mol}/RT), \qquad \text{(Eq 15)}$$

where $R = 8.3144621$ (J/mol/K) and T absolute temperature [K].The pre-exponential factor and the activation energy value are affected by the contact surface between the boriding medium and the substrate. The growth kinetics of Fe_2B layers proposed by the diffusion model was also verified by estimating the Fe_2B layer thicknesses as a function of temperature and exposure time. Fig. 14 shows the optical micrograph of the cross section of Armco iron sample borided at 1253 K for 5 h.

Table 2 shows a comparison of the boron activation energies in case of borided Armco iron substrates. The boron activation energy was estimated as equal to 157.5 kJ/mol for the borided Armco iron. The boride layer thickness can be evaluated from Eq 16 as follows:

$$v = \sqrt{\frac{17 D_{Fe_2B} t}{2500}}. \qquad \text{(Eq 16)}$$

Table 3 compares the experimental value of Fe_2B layer thickness obtained from Eq 16 at a temperature of 1253 K for 5 h with the simulated value of Fe_2B layer thickness for the

borided sample. A good agreement is then observed between the experimental data and the simulation results as depicted in Table 3. An iso-thickness diagram can be established based on Eq 16 by varying the boriding parameters as shown in Fig. 15.

6. Discussions

The Armco iron samples were pack borided in the temperature range of 1123-1273 K to study the formation of Fe_2B layers for a treatment time varying from 2 to 8 h. The microstructural observations revealed the presence of a single boride layer (Fe_2B) with a saw-tooth morphology in the all borided samples. It is also seen that the boride layer thickness changes with the boriding time. It indicates that the pack-boriding process is a diffusion-controlled phenomenon. The diffusion front increases for a prolonged treatment time. The boride layer thickness obtained at 1273 K reached a value of 244.02 ± 16.35 μm for 8 h of treatment, while it was only 109.47 ± 14.15 μm for 2 h.

This particular morphology promotes a good adhesion to the substrate. The iron boride formed at the surface of borided Armco iron at 1273 K for 8 h was verified by XRD analysis. The growth of Fe_2B layer has a highly anisotropic nature. So, the [001] crystallographic direction is the easiest path for the boron diffusion in the Fe_2B phase, because of the tendency of boride crystals to grow along a direction of minimum resistance, perpendicular to the external surface. As the metal surface is covered, an increasing number of Fe_2B crystals comes in contact with adjacent crystals and are forced to grow in the direction of material substrate, retaining an acicular shape (Ref 27). The cohesion strength quality of the Fe_2B layer formed at the surface of Armco iron was found to be related to HF4 standard for the Armco iron borided at 1273 K for 4 h of treatment.

In fact, the cohesion of the boride layer on the substrate depends on the boriding parameters. In this context, Taktak and Tasgetiren (Ref 36) have used the Rockwell-C cohesion test to study the cohesion of boride layers grown on H13 and AISI 304 steels. They found that their adhesion decreased with an increase of boriding time and temperature.

Using the diffusion model, the boron activation energy was estimated as equal to 157.5 kJ/mol for the borided Armco iron. The obtained value was compared with the literature data. The reported values listed in Table 2 are very close in case of the solid boriding (Ref 10, 12, 37) but different when using the gas boriding process (Ref 38, 39). In fact, the discrepancy in boron activation energies indicates that the rate-determining steps in powder and paste boriding deviate from that for gas boriding. Since gas boriding has the lowest activation energy, and provides values comparable with the diffusion of interstitials in iron-based lattices, it is suggested that powder and paste boriding experience an additional step. It is seen that the estimated values of boron activation energies depended on the nature of boriding agent.

An Iso-thickness diagram was plotted to be used as a simple tool to predict the Fe_2B layer thickness as a function of the boriding parameters (temperature and time). Hence, Eq 16 can be used to estimate the optimum thickness of Fe_2B layers for the borided Armco iron. The boride layer thickness is selected according to the requirements imposed by practical utilization of the borided material. As a rule, thin layers (e.g., 15-20 μm) are used to protect against adhesive wear (such as chipless shaping and metal stamping dies and tools), whereas thick layers are recommended to combat abrasive wear (extrusion tooling for plastics with abrasive fillers and pressing tools for the ceramic industry). In the case of low-carbon steels and low-alloy steels, the optimum boride layer thicknesses range from 50 to 250 μm, and for high-alloy steels, the optimum boride layer thicknesses are between 25 and 76 μm.

7. Conclusions

In this work, the boron diffusion coefficient in the Fe_2B layers grown on the Armco iron substrate was evaluated in the temperature range of 1123-1273 K using a kinetic model.

This model was based on the mass balance equation at the (Fe_2B/substrate) interface by considering the occurrence of boride incubation time.

The boron activation energy was estimated as equal to 157.5 kJ/mol when pack boriding the Armco iron substrate in the temperature range of 1123-1273 K. This value was in a good agreement with the data available in the literature.

Furthermore, the present model was validated by comparing the experimental value of Fe_2B layer thickness with the predicted one at a temperature of 1253 K during 5 h of treatment.

The cohesion strength quality of the boride layer formed at the surface of Armco iron was found to be related to HF4 standard for the Armco iron borided at 1273 K for 4 h of treatment.

Iso-thickness diagram was established as a simple tool to predict the Fe_2B layer thickness as a function of the boriding parameters (temperature and time).

Acknowledgments

The work described in this paper was supported by a grant of CONACyT and PROMEP México. Also, the authors want to thank to Ing. Martín Ortiz Granillo, who is in charge as Director of the Escuela Superior de Ciudad Sahagún which belongs to the Universidad Autónoma del Estado de Hidalgo, México, for all the facilities to accomplish this research work.

References

1. A.K. Sinha, Boriding (boronizing). in *ASM Int. Handbook*, Materials Park, OH, USA, 4, 1991, p. 437
2. G. Celebi, M. Ipek, C. Bindal, and A.H. Ucisik, Some Mechanical Properties of Borides Formed on AISI, 8620 Steel, *Mater. Forum*, 2005, **29**, p 456–460
3. O. Ozdemir, M.A. Omar, M. Usta, S. Zeytin, C. Bindal, and A.H. Ucisik, An Investigation on Boriding Kinetics of AISI, 316 Stainless Steel, *Vacuum*, 2008, **83**, p 175–179
4. M. Keddam and S.M. Chentouf, A Diffusion Model for Describing the Bilayer Growth (FeB/Fe_2B) During the Iron Powder-Pack Boriding, *Appl. Surf. Sci.*, 2005, **252**, p 393–399
5. W. Fichtl, Boronizing and Its Practical Applications, *Mater. Eng.*, 1981, **2**, p 276–286
6. I. Campos-Silva, M. Ortiz-Domínguez, M. Keddam, N. López-Perrusquia, A. Carmona-Vargas, and M. Elías-Espinosa, Kinetics of the Formation of Fe_2B Layers in Gray Cast Iron: Effects of Boron Concentration and Boride Incubation Time, *Appl. Surf. Sci.*, 2009, **255**, p 9290–9295

7. P.A. Dearnly and T. Bell, Engineering the Surface with Boron Based Materials, *Surf. Eng.*, 1985, **1**, p 203–217
8. J.R. Davis, *Surface Hardening of Steels: Understanding the Basics*, 1st ed., ASM International, USA, 2002
9. Z. Nait Abdellah, M. Keddam, and A. Elias, Evaluation of the Effective Diffusion Coefficient of Boron in the Fe_2B Phase in the Presence of Chemical Stresses, *Int. J. Mater. Res.*, 2013, **104**, p 260–265
10. C.M. Brakman, A.W.J. Gommers, and E.J. Mittemeijer, Boriding of Fe and Fe-C, Fe-Cr, and Fe-Ni alloys. Boride-Layer Growth Kinetics, *J. Mater. Res*, 1989, **4**, p 1354–1370
11. I. Campos-Silva, M. Ortiz-Domínguez, N. López-Perrusquia, A. Meneses-Amador, R. Escobar-Galindo, and J. Martínez-Trinidad, Characterization of AISI, 4140 Borided Steels, *Appl. Surf. Sci.*, 2010, **256**, p 2372–2379
12. I. Campos-Silva, M. Ortiz-Dominguez, H. Cimenoglu, R. Escobar-Galindo, M. Keddam, M. Elias-Espinosa, and N. López-Perrusquia, Diffusion Model for Growth of Fe_2B Layer in Pure Iron, *Surf. Eng.*, 2011, **27**, p 189–195
13. I. Campos, O. Bautista, G. Ramírez, M. Islas, J. De La Parra, and L. Zúñiga, Effect of Boron Paste Thickness on the Growth Kinetics of Fe_2B Boride Layers During the Boriding Process, *Appl. Surf. Sci.*, 2005, **243**, p 429–436
14. M. Keddam, Computer Simulation of Monolayer Growth Kinetics of Fe_2B Phase During the Paste-Boriding Process: Influence of the Paste Thickness, *Appl. Surf. Sci.*, 2006, **253**, p 757–761
15. M. Keddam, M. Ortiz-Domínguez, I. Campos-Silva, and J. Martínez-Trinidad, A Simple Model for the Growth Kinetics of Fe_2B Iron Boride on Pure Iron Substrate, *Appl. Surf. Sci.*, 2010, **256**, p 3128–3132
16. M. Keddam and R. Chegroune, A Model for the Growth of Fe_2B Layers on a Steel Substrate: Effect of the Surface Boron Concentration, *Solid State Phenom.*, 2011, **170**, p 185–189
17. Z. Nait Abdellah, M. Keddam, R. Chegroune, B. Bouarour, H. Lillia, and A. Elias, Simulation of the Boriding Kinetics of Fe_2B Layers on Iron Substrate by Two Approaches, *Matériaux et Techniques*, 2012, **100**, p 581–588
18. M. Keddam, A Kinetic Model for the Borided Layers by the Paste-Boriding Process, *Appl. Surf. Sci.*, 2004, **236**, p 451–455
19. I. Campos-Silva, N. López-Perrusquia, M. Ortiz-Domínguez, U. Figueroa- López, O.A. Gómes-Vargas, A. Meneses-Amador, and G. Rodríguez-Castro, Characterization of Boride Layers Formed at the Surface of Gray Cast Irons, *Kovove Mater.*, 2009, **47**, p 1–7
20. I. Campos-Silva, M. Ortiz-Domínguez, N. López-Perrusquia, R. Escobar-Galindo, O.A. Gómez-Vargas, and E. Hernández-Sánchez, Determination of Boron Diffusion Coefficients in Borided Tool Steels, *Defect Diffus. Forum*, 2008, **283–286**, p 681–686
21. L.G. Yu, X.J. Chen, K.A. Khor, and G. Sundararajan, FeB/Fe_2B Phase Transformation During SPS Pack-Boriding: Boride Layer Growth Kinetics, *Acta Mater.*, 2005, **53**, p 2361–2368
22. T.B. Massalski, *Binary Alloy Phase Diagrams*, 2nd ed., ASM International, Materials Park, OH, 1990, p 280
23. H. Okamoto (B-Fe) (boron-iron, *J. Phase Equilib. Diffus.*, 2004, **25**, p 297–298
24. V.I. Dybkov, *Reaction Diffusion and Solid State Chemical Kinetics*, 2nd ed., Trans Tech Publications, Switzerland, 2010, p 7
25. W. Jost, *Diffusion in Solids, Liquids, Gases*, Academic Press Inc, New York, 1960, p 69–72
26. P. Shewmon, *Diffusion in Solids*, 2nd ed., Minerals, Metals and Materials Society, USA, 1989, p 40
27. C. Martini and G. Palombarini, Mechanism of Thermochemical Growth of Iron Borides on Iron, *J. Mater. Sci.*, 2004, **39**, p 933–937
28. A.J. Ninham and I.M. Hutchings, On the morphology of thermochemically produced Fe_2B/Fe interfaces, *J. Vacuum Sci. Technol.*, 1986, **4**, p 2827–2831
29. M. Carbucicchio and G. Palombarini, Surface Modifications for Mechanical Applications, *Hyperfine Interact.*, 1994, **83**, p 91–110
30. I. Campos, R. Torres, O. Bautista, G. Ramírez, and L. Zuñiga, Effect of Boron Paste Thickness on the Growth Kinetics of Polyphase Boride Coatings During the Boriding Process, *Appl. Surf. Sci.*, 2006, **252**, p 2396–2403
31. I. Campos-Silva, M. Ortiz-Domínguez, O. Bravo-Bárcenas, M.A. Doñu-Ruiz, D. Bravo-Bárcenas, C. Tapia-Quintero, and M.Y. Jiménez-Reyes, Formation and Kinetics of FeB/Fe_2B Layers and Diffusion Zone at the Surface of AISI, 316 Borided Steels, *Surf. Coat. Technol.*, 2010, **205**, p 403–412
32. I. Campos-Silva, D. Bravo-Bárcenas, A. Meneses-Amador, M. Ortiz-Domínguez, H. Cimenoglu, U. Figueroa-López, and J. Andraca-Adame, Growth Kinetics and Mechanical Properties of Boride Layers Formed at the Surface of the ASTM F-75 Biomedical Alloy, *Surf. Coat. Technol.*, 2013, **237**, p 402–414
33. Verein Deutscher Ingenieure Normen. VDI 3198. VDI-Verlag, Dusseldorf, 1991 p 1-8
34. N. Vidakis, A. Antoniadis, and N. Bilalis, The VDI, 3198 Indentation Test Evaluation of a Reliable Qualitative Control for Layered Compounds, *J. Mater. Process. Technol.*, 2003, **143–144**, p 481–485
35. S. Taktak, Some Mechanical Properties of Borided AISI, H13 and 304 Steels, *Mater. Des.*, 2007, **28**, p 1836–1843
36. S. Taktak and S. Tasgertiren, Identification of Delamination Failure of Boride Layer on Common Cr-Based Steels, *J. Mater. Eng. Perform.*, 2006, **15**, p 570–573
37. I. Campos, J. Oseguera, U. Figueroa, J.A. García, O. Bautista, and G. Kelemenis, Kinetic Study of Boron Diffusion in the Paste-Boriding Process, *Mater. Sci. Eng. A*, 2003, **352**, p 261–265
38. M. Kulka, N. Makuch, A. Pertek, and L. Maldzinski, Simulation of the Growth Kinetics of Boride Layers Formed on Fe During Gas Boriding in H_2-BCl_3 Atmosphere, *J. Solid State Chem.*, 2013, **199**, p 196–203
39. H. Planitz, G. Treffer, H. Konig, and G. Marx, *Neue Hutte*, 1982, **27**, p 228–230